nature geoscience

LETTERS

PUBLISHED ONLINE: 9 JANUARY 2011 | DOI: 10.1038/NGEO1052

Regionally differentiated contribution of mountain glaciers and ice caps to future sea-level rise

Valentina Radić[1,2]* and Regine Hock[2,3]

The contribution to sea-level rise from mountain glaciers and ice caps has grown over the past decades. They are expected to remain an important component of eustatic sea-level rise for at least another century[1,2], despite indications of accelerated wastage of the ice sheets[3–5]. However, it is difficult to project the future contribution of these small-scale glaciers to sea-level rise on a global scale. Here, we project their volume changes due to melt in response to transient, spatially differentiated twenty-first century projections of temperature and precipitation from ten global climate models. We conduct the simulations directly on the more than 120,000 glaciers now available in the World Glacier Inventory[6], and upscale the changes to 19 regions that contain all mountain glaciers and ice caps in the world (excluding the Greenland and Antarctic ice sheets). According to our multi-model mean, sea-level rise from glacier wastage by 2100 will amount to 0.124 ± 0.037 m, with the largest contribution from glaciers in Arctic Canada, Alaska and Antarctica. Total glacier volume will be reduced by 21 ± 6%, but some regions are projected to lose up to 75% of their present ice volume. Ice losses on such a scale may have substantial impacts on regional hydrology and water availability[7].

Mountain glaciers and ice caps include only a minor fraction of all water on Earth bound in glacier ice (<1%) compared with the Antarctic and Greenland ice sheets (>99%), but their retreat has dominated the eustatic sea-level contribution in the past century[1,8]. The Fourth Assessment Report of the Intergovernmental Panel on Climate Change[9] (IPCC) projects twenty-first-century global sea-level rise due to wastage of mountain glaciers and ice caps to range between 0.07 and 0.17 m for different initial ice volume estimates and emission scenarios. This corresponds roughly to one-third of total predicted sea-level rise. The IPCC's approach allows for changes in glacier area, but glacier hypsometry is not modelled explicitly and hence for any warming scenario glaciers would melt away completely rather than approach a new equilibrium at higher altitudes. Ref. 10 developed a geometric volume model that allows glaciers to reach a new equilibrium and used a statistical grid-based approach to calculate the global glacier volume changes. They project a sea-level rise until the end of the twenty-first century of 0.046 m and 0.051 m using temperatures from two global climate models (GCMs) forced by the A1B emission scenario[11]. However, ref. 10 excluded the mountain glaciers and ice caps in Greenland and Antarctica (that is, those ice masses that are physically disconnected from the ice sheets), which comprise 32% of the total volume of all mountain glaciers and ice caps on Earth[12]. The IPCC (ref. 9) projections include these ice masses in an *ad hoc* manner by adding arbitrarily 20% to the projections of the glaciers outside Greenland and Antarctica. Another study[1] found accelerating rates of mass loss from available glacier mass balance data between 1995 and 2005.

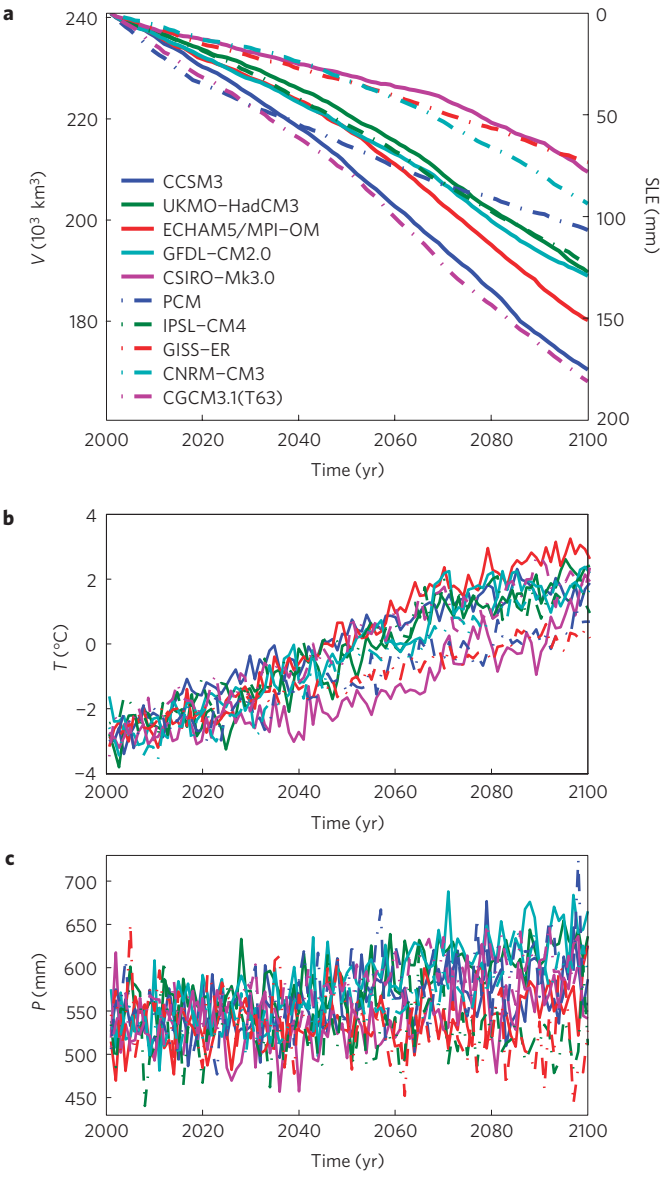

Figure 1 | Glacier volume evolutions in response to GCM projections. **a**–**c**, Projected volume, *V*, of all mountain glaciers and ice caps and corresponding SLE of the volume change for 2001–2100 (**a**), projections of annual mean temperature (**b**) and precipitation (**c**) from ten GCMs, where the values are averaged over all of the grid cells containing mountain glaciers and ice caps from the World Glacier Inventory (WGI-XF).

[1]Department of Earth and Ocean Sciences, University of British Columbia, Vancouver, British Columbia V6T 1Z4, Canada, [2]Geophysical Institute, University of Alaska, Fairbanks, Alaska 99775, USA, [3]Department of Earth Sciences, Uppsala University, 752 36 Uppsala, Sweden. *e-mail: vradic@eos.ubc.ca.

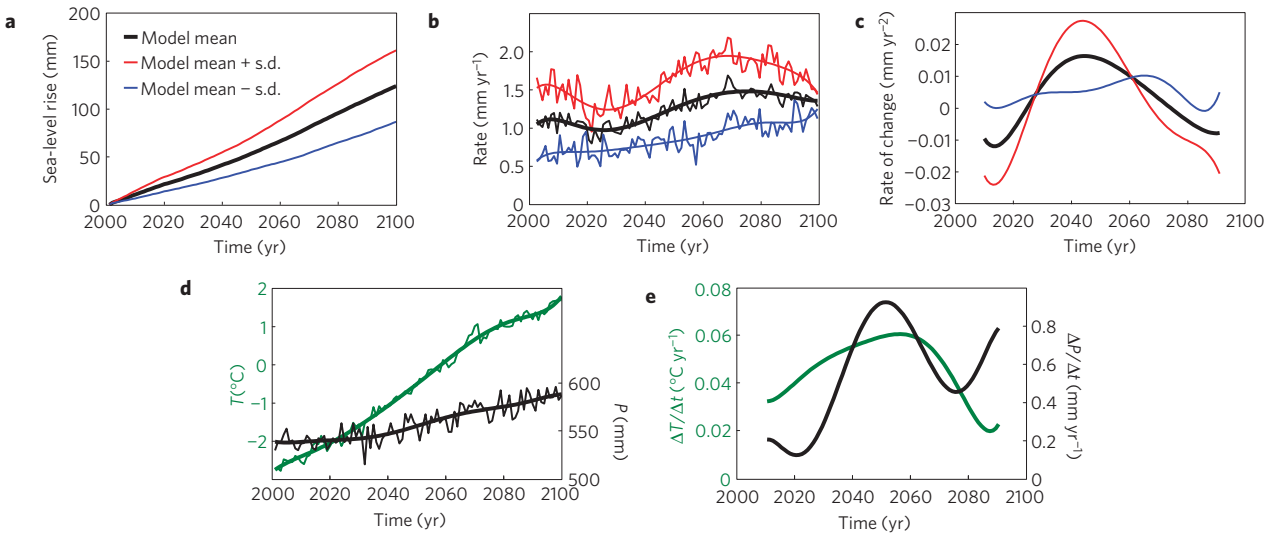

Figure 2 | Model projections for 2001–2100. a–e, Contribution of glacier wastage to sea-level rise, expressed in SLE (**a**), rate of sea-level rise including polynomial fit (**b**) and its rate of change (**c**), multi-model mean of annual temperature and precipitation projections (Fig. 1) including polynomial fit (**d**), and their annual rates of change (**e**). The black line in **a–c** denotes the model mean from 10 GCMs, red is the model mean + standard deviation and blue is the model mean − standard deviation. As the polynomial fit is not well constrained at the edges, the results for the first and last ten years in **c** and **e** are not shown.

Assuming this acceleration to remain constant over the twenty-first century, the projected total sea-level rise from all mountain glaciers and ice caps on Earth by 2100 is 0.240 ± 0.128 m (ref. 1), much larger than the one suggested by the IPCC (ref. 9) and especially by ref. 10. Assuming no acceleration, the projected sea-level rise drops to 0.104 ± 0.025 m (ref. 1), which is still considerably larger than the one in ref. 10. This indicates large discrepancies among the few available twenty-first century projections of mass loss by mountain glaciers and ice caps on a global scale (Supplementary Table S1). In addition, none of these estimates includes the effects of changing precipitation or provides regionally differentiated projections.

Here we project volume changes of all mountain glaciers and ice caps on Earth, spatially resolved for 19 glacierized regions, in response to twenty-first-century temperature and precipitation projections from ten GCMs (Supplementary Table S2) that were included in the IPCC report[9]. First we calibrate an elevation-dependent surface mass balance model with available mass balance observations worldwide (see the Methods section). Specifically, we use observed seasonal mass balance profiles[13–15] from 36 glaciers (Supplementary Table S3), and area-averaged mass balance estimates for 41 glacier regions[14] compiled from more than 300 glaciers with available observations between 1961 and 2004 (Supplementary Table S4). The latter are used as reference values for the initialization of our model, that is, to obtain initial mass balances for our future projections (Supplementary Methods). The model is forced by gridded climate data: monthly near-surface air temperature data from ERA-40 reanalysis[16] and a precipitation climatology[17] (see the Methods section). For the set of 36 glaciers with observed seasonal mass balance profiles we carry out multiple regressions between the calibrated model parameters and variables from the gridded climate data. The result is a set of transfer functions that allow us to assign parameter values to any glacier in the world on the basis of its climatic setting (Supplementary Table S5). The model is then applied to each individual mountain glacier and ice cap (with area ≥ 0.01 km^2) available in the recently updated and extended World Glacier Inventory[6] (WGI-XF), in total 120,229 mountain glaciers and 2,638 ice caps, henceforth referred to as WGI-XF glaciers. The total area of these glaciers covers roughly 40% of the global mountain glacier and ice cap area (317,724 km^2 out of 741,448 km^2, ref. 12).

To quantify future volume changes, we run the calibrated mass balance model for all WGI-XF glaciers with downscaled monthly twenty-first-century temperature and precipitation from ten GCMs, based on the widely used mid-range greenhouse emission scenario A1B (see the Methods section). As glaciers lose mass owing to temperature increase, they retreat and hence their hypsometry changes. We use volume–area–length scaling[18,19] to account for these changes and their feedbacks to glacier mass balance (for example, area-averaged mass loss may slow down as the glacier retreats from low-lying, high-ablation altitudes), allowing receding glaciers to approach a new equilibrium in a warming climate.

We present our volume projections for 19 glacierized regions (Supplementary Fig. S1), each containing a subset of WGI-XF glaciers. For nine of these regions the glacier inventory (WGI-XF) is incomplete, with the largest inventory gaps in Antarctica, Greenland and North America[12]. In these nine regions, we upscale the future volume changes with a scaling relation between the regional ice volume change and regional glacierized area (see the Methods section). The initial ice volumes for all 19 regions are taken from a recent study[12] where the global mountain glacier and ice cap volume was found to be 0.60 ± 0.07 m sea-level equivalent (SLE).

All projections for the twenty-first century show substantial mountain glacier and ice cap volume losses (Fig. 1a). However, results are highly sensitive to the choice of the forcing GCM. Volume losses range from 12 to 30%, corresponding to 0.07–0.18 m SLE. All ten GCMs unanimously project an increase in annual mean temperatures averaged over all grid cells containing WGI-XF glaciers (3.1–6.6 K), and the annual precipitation increases for most but not all GCMs (8% precipitation decrease to 21% increase) (Fig. 1b,c).

To compare our results with those of ref. 10, we exclude the mountain glaciers and ice caps in Greenland and Antarctica. For the GCM run common to both studies (GFDL-CM2.0), we arrive at a much higher projection for the twenty-first-century sea-level rise (0.096 m SLE) than ref. 10 (0.046 m SLE). This is probably due to the larger temperature sensitivity of our model owing to differences in model design and calibration as well as differences in model initialization. Whereas we initialize the model for each of the 41 glacier regions[14] individually (Supplementary Methods,

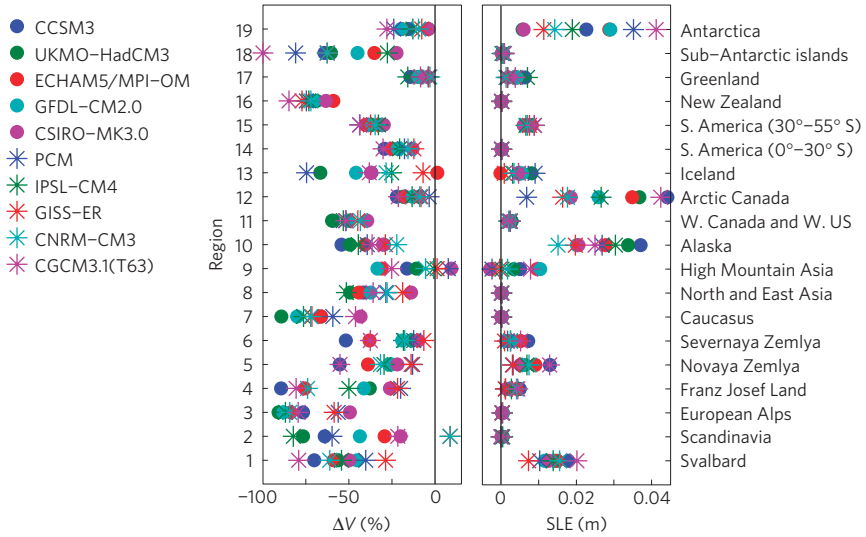

Figure 3 | Regional twenty-first-century glacier volume change. Volume change, ΔV, expressed in per cent from initial volume in year 2000 and in SLE. Results are presented for 19 regions based on temperature and precipitation projections from ten GCMs.

Table S4), ref. 10 used a globally uniform parameter adjustment as the final calibration step. Furthermore, our total initial volume for these glaciers (0.41 m SLE; ref. 12) is larger than in ref. 10 (0.241 m SLE). For all ten GCMs, the projected global volume loss for all glaciers outside Greenland and Antarctica ranges from 0.060 to 0.136 m SLE.

Assuming that future temperature and precipitation projections from all ten GCMs are equally credible, we calculate a multi-model mean for global volume loss by 2100 of 0.124 ± 0.037 m SLE, where the uncertainty range is ± 1 standard deviation (Fig. 2a). According to the multi-model mean, the volume loss rate varies between 0.9 ± 0.4 mm SLE yr^{-1} and 1.6 ± 0.4 mm SLE yr^{-1} during the twenty-first century (Fig. 2b), and the volume loss acceleration peaks at 0.016 ± 0.010 mm SLE yr^{-2} in the 2040s (Fig. 2c). Multi-model means of annual temperature and precipitation (Fig. 2d), and their rates of change (Fig. 2e), depict the temperature as a dominant driver of our modelled glacier volume changes. Hence, the decline in the rate of temperature rise around 2060 is followed by a decline in the rate of volume loss. When averaged over 2002–2006, the projected volume loss rate of 1.1 ± 0.4 mm SLE yr^{-1} closely matches the estimated rates of recent mountain glacier and ice cap contribution to sea-level rise[1,2].

Volume change (as % of initial volumes) varies considerably among the 19 regions and among the GCMs (Fig. 3, Supplementary Table S6). The multi-model mean ranges between 8 and 75% volume loss, with the smallest values in Greenland (8 ± 4%) and High Mountain Asia (10 ± 16%), and the largest values in the European Alps (75 ± 15%) and New Zealand (72 ± 7%). Despite the large relative volume loss in the last two regions, their contribution to sea-level rise is negligible owing to the small total ice volume. The main contributors to global mountain glacier and ice cap shrinkage by 2100 are Arctic Canada (0.027 ± 0.012 mSLE), Alaska (0.026 ± 0.007 m SLE), Antarctica (0.021 ± 0.012 m SLE), Svalbard (0.014 ± 0.004 m SLE) and the Russian Arctic (Franz Josef Land, Novaya Zemlya and Severnaya Zemlya; 0.013 ± 0.003 m SLE). The largest scatter of volume projections among the ten GCMs is found in Scandinavia (from 83% volume loss to 9% volume gain by 2100), the sub-Antarctic islands (22–100% volume loss) and Franz Joseph Land (20–89% volume loss). This is mainly caused by high mass balance sensitivities to temperature and/or precipitation changes of these regions and by the large range in temperature and/or precipitation projections.

A major uncertainty in our estimates arises from the initialization of our model to previously reported spatially differentiated mass balance estimates[14]. According to the reported standard errors in the reference area-averaged mass balance estimates[14], we assume an error range of ± 0.15 m yr^{-1} for each glacier region (equivalent to ± 0.31 mm SLE yr^{-1} in globally averaged mass balance). Reinitializing the model with the lower bound estimates for each of the 41 glacier subregions, the projected multi-model mean for the twenty-first-century volume loss is 0.103 ± 0.037 m SLE. For the upper bound initialization, the projected volume loss is 0.142 ± 0.037 m SLE. We also quantify the uncertainties due to biases in the model input data, model calibration and scaling methods (Supplementary Methods, Figs S2, S3), and show that the errors lie within the range of ± 0.04 m SLE for the global volume change by 2100. Further uncertainties are discussed in Supplementary Methods.

Our projected sea-level rise from glacier wastage is probably a lower bound because only the surface mass balance is modelled, neglecting any mass loss by iceberg calving of marine-terminating glaciers. Studies on marine-terminating ice caps[20,21] have shown that calving may account for roughly 30–40% of total mass loss, and hence constitutes a significant contributor to mass loss, especially in polar environments where many glaciers terminate in the sea. However, owing to the scarcity of estimates and the complexity in modelling iceberg calving, this component to mass loss is still neglected in global-scale mass balance modelling of mountain glaciers and ice caps[9,10,22,23].

Our range of projected twenty-first-century volume loss forced by ten GCMs and the A1B emission scenario is similar to the IPCC (ref. 9) range based on an ensemble of GCMs. In addition, our spatially differentiated projections reveal the main regional contributors to sea-level rise as well as the regions most vulnerable to glacier wastage. Many of these glacierized regions are still facing large uncertainties in the climate projections due to the choice of GCM. On a global scale, less than half of the mountain glacier and ice cap volume will have disappeared by the end of the twenty-first century. Therefore, glaciers other than the ice sheets will continue to be an important contributor to sea-level rise and watershed hydrology, if warming continues beyond 2100 as is expected[9].

Methods

For each WGI-XF glacier, monthly melt (in metres water equivalent) is calculated through a degree-day model that differentiates between degree-day factors for snow

and for ice (Supplementary Methods). Monthly snow accumulation is obtained from a threshold temperature that differentiates between snow and rain. Refreezing is parameterized as a function of annual mean air temperature[24]. Mass balance calculations are carried out for 20 m elevation bands.

We tune the model parameters to yield maximum agreement between (1) times series of modelled and observed area-averaged winter and summer mass balance, and (2) series of modelled and observed winter and summer mass balance along glacier elevation, averaged over the period of observations. The tuning is carried out for each individual glacier in the subset of 36 glaciers. Modelled area-averaged mass balances, B (in kg m^{-2}), are converted into SLE by:

$$\mathrm{SLE} = -\frac{BS}{\rho S_{\mathrm{ocean}}}$$

where S is the glacierized area, ρ is the density of water and S_{ocean} is the area of the ocean (362×10^{12} m^2).

The area–altitude distribution of each WGI-XF glacier is approximated from the available data in WGI-XF (ref. 6) on surface area, length and glacier elevation range (minimum and maximum elevation) following the approach of ref. 10: for mountain glaciers, the area–altitude distribution is approximated with a linearly increasing function from the terminus to the mean altitude and a linearly decreasing function above (Supplementary Fig. S4). This approximation relies on the argument that observed area–altitude distributions tend to have a maximum near the mean altitude where the mass flux of ice is greatest. The distribution for ice caps, assuming perfect plasticity, is approximated by a parabolic shape with a circular base[25] (Supplementary Fig. S4). If the elevations are not reported in the WGI, we derive these from the 30-arc-sec (1-km) gridded, quality-controlled digital elevation model of the Global Land One-kilometre Base Elevation (GLOBE) project[26]. The elevations from GLOBE are extracted by finding maximum and minimum elevations within the range of 1/48°(~2.5 km) from a glacier. The sensitivity of our volume projections to the biases in these data is tested and shown to lie within the error range of ±0.04 m SLE for the global volume change by 2100 (Supplementary Methods).

As GCMs are unable to represent the local subgrid-scale features and dynamics, this leads to biases in the climate variables over the local glacier scale. Following a statistical downscaling approach[27], we shift the future monthly temperature time series for each GCM grid cell containing WGI-XF glaciers by the average bias for each month between the GCM and ERA-40 temperatures over the period 1980–1999. Annual precipitation in the GCM is scaled with a correction factor between precipitation climatology[17] and GCM mean precipitation over 1980–1999.

After deriving the volume projections for all WGI-XF glaciers we upscale the projections for nine glacierized regions with an incomplete glacier inventory. We assume that in each of these regions the ratio of volume change of all WGI-XF glaciers and the total volume change is equal to the ratio of the area of all WGI-XG glaciers and total initial glacierized area. This upscaling relation serves as a good first-order approximation, as tested on the ten regions with complete glacier inventories (Supplementary Methods, Fig. S3).

Received 30 March 2010; accepted 26 November 2010; published online 9 January 2011

References

1. Meier, M. F. *et al.* Glaciers dominate eustatic sea-level rise in the 21st century. *Science* **317,** 1064–1067 (2007).
2. Cogley, J. G. Geodetic and direct mass-balance measurements: Comparison and joint analysis. *Ann. Glaciol.* **50,** 96–100 (2009).
3. Rignot, E. & Kanagaratnam, P. Changes in the velocity structure of the Greenland ice sheet. *Science* **311,** 986–990 (2006).
4. Allison, I., Alley, R. B., Fricker, H. A., Thomas, R. H. & Warner, R. C. Ice sheet mass balance and sea level. *Antarct. Sci.* **21,** 413–426 (2009).
5. Cazenave, A. *et al.* Sea level budget over 2003–2008: A reevaluation from GRACE space gravimetry, satellite altimetry and Argo. *Glob. Planet. Change* **65,** 83–88 (2009).
6. Cogley, J. G. A more complete version of the world glacier inventory. *Ann. Glaciol.* **50,** 32–38 (2009).
7. Hock, R., Jansson, P. & Braun, L. in *Global Change and Mountain Regions—A State of Knowledge Overview* (eds Huber, U. M., Reasoner, M. A. & Bugmann, H.) (Springer, 2005).
8. Lemke, P. *et al.* in *IPCC Climate Change 2007: The Physical Science Basis* (eds Solomon, S. *et al.*) (Cambridge Univ. Press, 2007).
9. Meehl, G. A. *et al.* in *IPCC Climate Change 2007: The Physical Science Basis* (eds Solomon, S. *et al.*) (Cambridge Univ. Press, 2007).
10. Raper, S. C. B. & Braithwaite, R. J. Low sea level rise projections from mountain glaciers and ice caps under global warming. *Nature* **439,** 311–313 (2006).
11. Nakićenović, N. & Sward, R. (eds) *Special Report on Emission Scenarios* 570–599 (Cambridge Univ. Press, 2000).
12. Radić, V. & Hock, R. Regional and global volumes of glaciers derived from statistical upscaling of glacier inventory data. *J. Geophys. Res.* **115,** F01010 (2010).
13. Dyurgerov, M. B. *Glacier Mass Balance and Regime: Data of Measurements and Analysis*, INSTAAR Occasional Paper No. 55 (2002).
14. Dyurgerov, M. B. & Meier, M. F. *Glaciers and the Changing Earth System: A 2004 Snapshot*. Occasional Paper 58, Institute of Arctic and Alpine Research, (Univ. Colorado, 2005).
15. Heaberli, W. *et al. Fluctuations of Glaciers*, 1995–2000, Vol. 8 (Intl. Comm. on Snow and Ice, Intl. Assoc. of Hydrol. Sci./UNESCO, 2005).
16. Kållberg, P. W., Simmons, A. J., Uppala, S. M. & Fuentes, M. *The ERA-40 Archive*. ERA-40 Project Report Series 17, (ECMWF, 2004).
17. Beck, C., Grieser, J. & Rudolf, B. *A New Monthly Precipitation Climatology for the Global Land Areas for the Period 1951 to 2000*. Climate Status Report 2004, (German Weather Service, 2005).
18. Bahr, D. B., Meier, M. F. & Peckham, S. D. The physical basis of glacier volume–area scaling. *J. Geophys. Res.* **102,** 20355–20362 (1997).
19. Radić, V., Hock, R. & Oerlemans, J. Analysis of scaling methods in deriving future volume evolutions of valley glaciers. *J. Glaciol.* **54,** 601–612 (2008).
20. Burgess, D., Sharp, M., Mair, D., Dowdeswell, J. & Benham, T. Flow dynamics and iceberg calving rates of Devon Ice Cap, Nunavut, Canada. *J. Glaciol.* **51,** 219–230 (2005).
21. Dowdeswell, J. A., Benham, T. J., Strozzi, T. & Hagen, O. Iceberg calving flux and mass balance of the Austfonna ice cap on Nordaustlandet, Svalbard. *J. Geophys. Res.* **113,** F03022 (2008).
22. Kaser, G., Cogley, J. G., Dyurgerov, M. B., Meier, M. F. & Ohmura, A. Mass balance of glaciers and ice caps: Consensus estimates for 1961–2004. *Geophys. Res. Lett.* **33,** L19501 (2006).
23. Hock, R., de Woul, M., Radić, V. & Dyurgerov, M. Mountain glaciers and ice caps around Antarctica make a large sea-level rise contribution. *Geophys. Res. Lett.* **36,** L07501 (2009).
24. Woodward, J., Sharp, M. & Arendt, A. The influence of superimposed-ice formation on the sensitivity of glacier mass balance to climate change. *Ann. Glaciol.* **24,** 186–190 (1997).
25. Paterson, W. S. B. *The Physics of Glaciers* 3rd edn (Elsevier, 1994).
26. The Global Land One-kilometer Base Elevation (GLOBE) (Digital Elevation Model, Version 1.0. National Oceanic and Atmospheric Administration, National Geophysical Data Center, http://www.ngdc.noaa.gov/mgg/topo/globe.html, 1999).
27. Radić, V. & Hock, R. Modelling mass balance and future evolution of glaciers using ERA-40 and climate models – A sensitivity study at Storglaciären, Sweden. *J. Geophys. Res.* **111,** F03003 (2006).

Acknowledgements

We thank A. Rasmussen, F. Anslow, A. Arendt, M. Haseloff and M. Truffer for comments on the manuscript. Mass balance data were provided by M. de Woul, M. Dyurgerov and J. Shea. The Arctic Region Supercomputing Center at the University of Alaska provided computing resources. Funding was provided by FORMAS, Sweden (project 21.4/2005-0387).

Author contributions

V.R. led the development of this study, prepared all data sets and carried out all calculations. R.H. initiated the study and contributed to the development of the methodology, discussion of results and the writing of the manuscript.

Additional information

The authors declare no competing financial interests. Supplementary information accompanies this paper on www.nature.com/naturegeoscience. Reprints and permissions information is available online at http://npg.nature.com/reprintsandpermissions. Correspondence and requests for materials should be addressed to V.R.

nature geoscience

SUPPLEMENTARY INFORMATION

DOI: 10.1038/NGEO1052

Regionally differentiated contribution of mountain glaciers and ice caps to future sea-level rise

Valentina Radić * and Regine Hock

Supplementary Methods

1. Mass balance model

For each elevation band of a glacier and each month we calculate the specific mass balance, *b, as*

$$b = a + c + R\,, \tag{1}$$

where a represents ablation (mass loss is defined negatively), c accumulation and R refreezing. Ablation is calculated through a degree-day model. Thus ablation, a (mm w.e.), is calculated for each elevation band as

$$a = f_{ice/snow} T_m^+ n\,, \tag{2}$$

where $f_{ice/snow}$ is a degree-day factor for ice or snow (mm w.e. d^{-1} $°C^{-1}$), T_m^+ (°C) is a positive monthly mean temperature and n is the number of days in a month m. The degree-day factor for snow, f_{snow} is used above the equilibrium line altitude (ELA) regardless of snow cover, while below the ELA we apply f_{ice} when snow depth is zero. The ELA is calculated from the observed annual mass balance profiles averaged over the observational period and is kept constant in time for the calibration period. For the future projections ELA is set to the mean glacier height and is time dependent since glacier volume, area and length are time dependent (volume-area-length scaling). Monthly snow accumulation, c (mm w.e.), is calculated for each elevation band as

$$c = \delta_m P_m \quad \begin{cases} \delta_m = 1, T_m < T_{snow} \\ \delta_m = 0, T_m \geq T_{snow} \end{cases}, \tag{3}$$

where P_m is monthly precipitation (mm) which is assumed to be snow if the monthly temperature T_m (°C) is below the threshold temperature, T_{snow}, which discriminates snow from rain precipitation. Annual refreezing, R (cm), is related to the annual mean air temperature, T_a (°C), as[24]

$$R = -0.69 T_a + 0.0096\,, \tag{4}$$

where the lower boundary for R is 0 across the whole glacier, while an upper boundary is applied in the ablation zone and assumed equal to the accumulated snow. Monthly melt is considered to refreeze until the accumulated melt in one balance year exceeds the potential refreezing, R.

To correct for the bias in temperature input we apply a 'statistical lapse rate', lr_{ERA}, between ERA-40 altitude of the grid cell containing the glacier, h_{ERA}, and the highest altitude of the glacier, h_{max}. From h_{max} to the snout of the glacier we apply another lapse rate, lr, to simulate the increase in temperature as elevation decreases along the glacier surface. The temperature, T, at each elevation band is calculated as

$$T = T_{ERA} + lr_{ERA}(h_{\max} - h_{ERA}) + lr(h - h_{\max})\,, \tag{5}$$

where h is the average altitude of the elevation band, and T_{ERA} is temperature from ERA-40 in the calibration period and downscaled GCM temperature in the period 2001-2100. Details on GCM downscaling are given under Methods in the main text and in ref. 27. Note that except for T_{ERA} all other variables are equal for the hindcast simulations using ERA-40 and the future simulations using GCM data.

We correct for the bias in precipitation by assigning a precipitation correction factor, k_P, to compute precipitation at h_{max} while from the top to the snout of the glacier we apply a precipitation

DOI: 10.1038/NGEO1052

gradient d_{prec} (% of precipitation increase per meter of elevation increase). Thus, the precipitation, P, at each elevation band is calculated as

$$P = k_P P_{ERA}\left[1 + d_{prec}(h - h_{\max})\right], \quad (6)$$

where P_{ERA} is precipitation from the precipitation climatology[17] in the calibration period and downscaled GCM precipitation in the period 2001-2100.

Area-averaged specific mass balance is computed by

$$B = \frac{\sum_{i=1}^{n} b_i S_i}{\sum_{i=1}^{n} S_i}, \quad (7)$$

where b_i and S_i are discrete values of mass balance and surface area, respectively, for each elevation band (i=1...n). Winter mass balance, B_w, and summer mass balance, B_s, are integrated over the winter and summer season, respectively. The beginning of winter (summer) season for glaciers located in the northern hemisphere north of 75°N is 1 September (1 May) otherwise it is 1 October (1 April), while for glaciers in the southern hemisphere it is 1 April (1 Oct).

2. Model calibration and initialization

For model calibration we use the observations of seasonal mass balance profiles available from 36 glaciers listed in Table S3. For model initialization we use area-averaged mass balance estimates for 41 glacier regions[14] listed in Table S4. These estimates were compiled from more than 300 glaciers with available observations (between 1961 to 2004), which were weighted by the surface area of individual glaciers and then by the aggregate surface area of the glacier region[14].

The model is calibrated by optimizing seven model parameters: lr_{ERA}, lr, f_{snow}, f_{ice}, k_P, d_{prec} and T_{snow} (Equations 2, 5, 6). We tune the parameters to yield maximum agreement (minimum root-mean-square error) between (1) times series of modelled and observed area-averaged winter and summer mass balance, and (2) series of modelled and observed winter and summer mass balance along glacier elevation, averaged over the period of observations. The optimization is performed independently for each individual glacier in Table S3. Since these glaciers do not experience large area changes in the reference period and since the observed area changes are not updated on a yearly basis we calculate 'reference surface mass balances' (ref. 28) assuming the reported glacier area constant in time.

To run the mass balance model on each glacier from the WGI-XF inventory we need to assign parameter values to each individual WGI-XF glacier. We use the following procedure to obtain the parameter values: for the set of 36 glaciers (Table S3) we perform multiple regressions between the calibrated model parameters and variables from the gridded climate data. We assume that model parameters vary between glaciers as a function of climatic setting. Previous studies[29,30] have shown that glaciers in a maritime climate with smaller annual temperature amplitude tend to be more sensitive to temperature and precipitations changes than sub-polar or continental glaciers with drier climate and larger temperature amplitude. Based on these findings we include the following variables in our regression analysis: annual precipitation (P_{ann}), continentality index (CI) defined as the average difference between the coldest and warmest mean monthly temperature during one year (e.g. ref. 31), mean glacier elevation ($\bar{h}$), elevation range and mass balance sensitivity to temperature and precipitation change. The mass balance sensitivities to 1 K temperature increase ($\Delta B/\Delta T$) and 10% precipitation increase ($\Delta B/\Delta P$) are derived from the mass balance model as

$$\frac{\Delta \overline{B}}{\Delta T} = \frac{\overline{B}(+1K) - \overline{B}}{1K}, \quad (8)$$

$$\frac{\Delta \overline{B}}{\Delta P} = \frac{\overline{B}(+10\%) - \overline{B}}{10\%}, \quad (9)$$

where $\overline{B}$ is modelled area-averaged annual mass balance averaged over the mass balance observational period while $\overline{B}(+1K)$ and $\overline{B}(+10\%)$ are modelled balances with uniformly perturbed temperature of +1K and precipitation of +10%, respectively. Continentality index, *CI* (K), and mean annual precipitation, P_{ann} (mm), are averaged over the period 1980-2000.

The resulting functions from the multiple regressions are presented in Table S5. Only three out of seven model parameters have significant correlations at the 95% confidence level with at least one of the variables. These functions are then used to obtain model parameters for each WGI–XF glacier. However, four out of seven parameters still remain undefined since no significant relations could be established with climate variables. For three of these parameters we assume that the mean value from the sample of 36 glaciers is a good first order approximation for all WGI-XF glaciers (Table S5). However, sensitivity experiments (see 3.1) showed that the model is sensitive to the choice of the remaining parameter (lr_{ERA}) because of the dominant role of temperature in controlling glacier mass balance. Therefore this parameter is constrained in a final calibration step using area-averaged mass-balances reported for 41 subregions[14]. The parameter is varied (by a constant step of 0.0001 K m^{-1}) for each subregion until these reference balances, averaged over the period for which annual balances have been reported, match the modelled balances for the same period within ±0.1 m w.e. yr^{-1}. This procedure is justified since our aim is not to hindcast regional mass balances but rather to obtain initial balances for our future projections.

Observations in the 41 subregions[14] range over varying time intervals between 1961 and 2000 and only seldom range over the entire period. Therefore, we calibrate our model only for the years where there actually is data. For glacier regions with insufficiently long data (<4 years) we use other available sources of observations (e.g. ref. 32 for Patagonia) or consider the estimate from the climatically most similar and geographically nearest glacier region as a representative estimate (details are given in Table S4). For the glacier region peripheral to the Antarctic ice sheet (glacier region 40 in Table S4) ref. 14 gives an estimate of -0.03 m yr^{-1} for the period 1971-1975. Tuning our model to this value for the same observational period and then calculating the mass balance for 1961-2000 resulted in -0.20 m yr^{-1}. Another study[23] reported an estimate of -0.60 ± 0.44 m yr^{-1} for the period 1961-2004. Here we chose a mid-range estimate of those two, -0.40 m yr^{-1}, to be our reference estimate for the period 1961-2000.

After model initialization the calibrated model is run for all 41 subregions for the entire period 1961-2000. Resulting mass balances for each glacier subregion are then aggregated into our 19 regions (Figure S1), providing regional and global area-averaged mass balances for 1961-2000 (Table S6). The modeled global mass balance for this period corresponds to 0.56 mm SLE yr^{-1} which agrees well with previous estimates[8,22] although higher values have been reported[23] though not for exactly the same period. For comparison with earlier studies, we calculate the mass balance sensitivity to a uniform 1 K temperature increase and 10% increase in precipitation, respectively. Our globally averaged mass balance sensitivities are -0.60 m yr^{-1} K^{-1} and +0.07 m yr^{-1}, and hence within the range of previously reported estimates[8,10].

To test the validity of the modelling approach we compare our modeled ice loss to the geodetically-derived ice loss of two regions where calving can be assumed small: Swiss Alps[33] and British Columbia[34]. Ref. 33 used two different methods for calculating the mean cumulative mass balance of the entire region of Swiss Alps. Their results yielded -7.0 m w.e. and -10.95 m w.e. of glacier thinning over the period 1985-1999. Running our mass balance model for all WGI-XF glaciers that belong to the same domain and the same period, we obtain a mean cumulative mass balance of -7.9 m w.e.. For the same period, ref. 34 quantified the thinning rate of all glaciers in

DOI: 10.1038/NGEO1052

British Columbia to be -0.78 ± 0.19 m yr^{-1}. Our model yields -0.96 m yr^{-1}, and hence results are within their error bounds. Thus, for both regions our estimates agree well with the published estimates derived from geodetic methods.

3. Analysis of the uncertainties

Here we quantify the uncertainties in the projected SLE by 2100 due to (1) model calibration, (2) volume-area-length scaling, (3) the biases in glacier area, (4) the upscaling of volume changes for the nine regions with incomplete glacier inventories and (5) the biases in the glacier elevation. Finally, we discuss the uncertainties which can not be quantified by a standard error analysis or a series of sensitivity tests, but which are known to affect the accuracy of global projections of SLE.

3.1 Uncertainties in the model calibration

We investigate the sensitivity of the mass balance model to the choice of parameter values (Table S3) considering that some of the model parameters could not be constrained by transfer functions (Table S5). First, we calculate the mean value for each model parameter by averaging its value across all 36 glaciers (Table S3). The model is then run with the optimized values for six parameters and the mean value for the remaining parameter. The results show that the highest root-mean square error (between model and observed area-average mass balance) occurs when the model is run with the mean value for lr_{ERA}, while the other parameters have their optimized values. This error is largest for the summer mass balance. Second highest root-mean square errors occur when the model is run with the mean value for f_{snow} and for the precipitation correction factor, k_p.

These experiments are then repeated for all WGI-XF glaciers and area-averaged annual mass balances are computed for the 41 glacier subregions[14] over the period 1961-2000. Results are most sensitive to the perturbation of lr_{ERA}. For some glacier regions, a perturbation of only $\Delta lr_{ERA} = \pm 0.01$ $K(100m)^{-1}$ changes the area-averaged mass balance of the glacier region by ±0.15 m yr^{-1}. For other regions, larger perturbation (up to ±0.17 $K(100m)^{-1}$) is needed to reach this error range. The sensitivity to this parameter is higher if a glacier region has larger mass balance sensitivity to temperature change. If lr_{ERA} is set to its original value derived from the model initialization while other model parameters are perturbed (e.g. using mean values from the sample of 36 glaciers instead of applying the transfer functions for f_{snow}, f_{ice} and k_P) the area-averaged mass balance across all the regions is still within ±0.15 m yr^{-1}. We conclude that the quantified errors due to the model calibration do not exceed ±0.15 m yr^{-1} (±0.31 mm SLE yr^{-1}) of global area-averaged mass balance.

Our sample of 36 glaciers used for the model calibration and derivation of the transfer functions (Table S5) is geographically biased with the majority of glaciers located in Scandinavia and southern Canada (Table S3). To evaluate the validity of our transfer functions to the regions with climatic conditions that are not represented by our sample, we perform the following analysis for Arctic Canada and High Mountain Asia. These regions represent climate types (cold/dry and monsoon) that are not included in our glacier sample. We plot annual precipitation of the WGI-XF glaciers versus continentality index *CI* (Fig. S2a, d), both variables representing independent variables in the transfer functions. We also plot the mass balance sensitivity to temperature change ($\Delta B/\Delta T$) versus *CI*, and mass balance sensitivity to precipitation change ($\Delta B/\Delta T$) versus P_{ann}. Fig. S2a illustrates that *CI* for the location of all WGI-XF glaciers of Arctic Canada is consistently larger than for the 36 calibration glaciers indicating that the latter glaciers fail to represent the strong continental conditions in the Canadian Arctic. However, modeled mass balances of all WGI-XF glaciers in the Canadian Arctic are less sensitive to temperature and precipitation changes than is the case for the 36 sample glaciers. To validate these results we add to the scatter plots the data from ref. 23 where the climatic conditions and mass balance sensitivities for 88 glaciers worldwide have been assessed. Four of these glaciers belong to Canadian Arctic (Baby, Devon Ice Cap, Meighen Ice Cap, and Melville South Ice Cap) and have $CI > 35$ K. As illustrated in Figure S2b and c, our scatter of modeled sensitivities is within the scatter of their estimates, providing confidence in the validity of our transfer functions beyond the range of climatic conditions they were derived for. The results for the High Mountain Asia (Fig. S2e-f) support this conclusion.

3.2 Uncertainties in the volume-area-length scaling

We use volume-area-length scaling (e.g. refs 18, 19) to estimate the changes in volume and hypsometry of each WGI-XF glacier. The values for scaling coefficients are taken from previous studies[12,35,36]. However, coefficients have been shown to vary widely between glaciers depending among other factors on geometry, slope, thermal regime and flow characteristics, and therefore the choice of scaling coefficients constitutes a major uncertainty[19]. For example a glacier with a relatively flat and thick glacier tongue may lose mass primarily through thinning while the area changes little, and hence the coefficients from previous studies may not hold. Also, coefficients for the same glacier can be expected to vary with time as the glacier retreats. Additionally, the performance of volume-area-length scaling in simulating the volume evolutions of glaciers (for example through comparison with results from ice-flow modeling) has only been sparsely investigated[19], and to our knowledge never for ice caps.

Following ref. 12 we perturb the scaling coefficients in order to assess the uncertainties in the final SLE estimates. Assuming the same error ranges in the scaling coefficients as in ref. 12, we rerun the volume projections using their upper and lower bound value. Projected global volume loss by 2100 is within the range of ±0.04 m SLE for each GCM.

3.3 Uncertainties in glacier area

We assess the uncertainties in the projections due to errors in glacier area. Because the measurement error for glacier area is generally not reported in WGI-XF, we assume it to be 10% for each individual glacier as previously assumed in ref. 12. Perturbing the area by ±10% for each WGI-XF glacier the error range in the global projections by 2100 does not exceed ±0.04 m SLE.

For the nine regions with incomplete glacier inventories we use the estimates for the total glacierized area per region from ref. 12. Allowing an error of ±10% in these estimates we arrive at the uncertainty range of ±0.01 m SLE in the global projections by the end of 2100. We note that the largest discrepancies in reported total glacierized area are for two regions in the North America: Alaska (with Yukon) and West Canada/West US. While our reference estimate[12] for Alaska (with Yukon) is 79,260 km^2, refs 14 and 37 report 85,150 km^2 and 87,860 km^2, respectively. The difference is within our assumed error range for glaciered area of ±10% per region. For West Canada and West US ref. 14 gives an estimate of 39,160 km^2, which is considerably larger than our areal estimate of 21,480 km^2 (ref. 12), while more recent assessments than ref. 14 give 26,728 km^2 for western Canada[38] (provinces of British Columbia and Alberta), and 688 km^2 for West US[39]. This is 28% more than our areal estimate[12], and hence above our allowed error range of ±10%. Assuming the latter estimate as an upper bound estimate, the projected SLE for the 21st century from that region increases from 2.4 mm to 3.6 mm.

3.4 Uncertainties in the upscaling of volume changes

After deriving the volume projections for all WGI-XF glaciers we upscale the projections for nine glacierized regions with incomplete glacier inventory. We assume that in each of these regions the ratio of volume change of all WGI-XF glaciers and total volume change $\Delta V_{WGI}/\Delta V_{region}$ is equal to the ratio of the area of all WGI-XF glaciers and the total initial glacierized area S_{WGI}/S_{region}. We test this assumption in the ten regions with complete glacier inventory by applying a Monte Carlo analysis of split-sample tests. Glaciers from each of the 10 regions are randomly sampled so that the samples contain 95% to 5% (decreasing by 5%) of the total number of glaciers in the region, thus simulating the cases of incomplete inventories. The sampling is repeated 100 times for each region. Results are illustrated for one GCM in Figure S3, but are similar for all GCMs. We fit the linear function to the scatter in Figure S3 and assume the standard error from the linear regression (e.g. ref. 40) to be a representative uncertainty in our upscaling of volume changes in nine regions with incomplete inventories. Propagating these standard errors in the global estimates, the final error bound for global volume loss until 2100, derived from ten GCMs, is ±0.038 m SLE.

DOI: 10.1038/NGEO1052

3.5 Biases in the glacier elevation data

Two of the input variables to our mass balance model are maximum and minimum glacier elevation. For 12% of the WGI-XF glaciers these variables are not reported in the inventory and therefore are extracted from the 30-arc-second (1-km) gridded, quality-controlled Digital Elevation Model (DEM) of the Global Land 1-km Base Elevation (GLOBE) Project[26]. In only six out of the 41 subregions used for model initialization more than 10% of the WGI-XF glaciers lack elevation data. These regions are: Pamir (26%), Svalbard (77%), Polar Ural (59%), Severnaya Zemlya (81%), Franz Josef Land (95%) and South America II (26%). As a sensitivity experiment, we use the elevations from GLOBE DEM for each WGI-XF glacier in these regions. We also include a well-inventoried region (Novaya Zemlya; with only 7% WGI-XF glaciers lacking elevation data) in this sensitivity experiment. Differences between the maximum/minimum elevation from the glacier inventory and the corresponding elevations from GLOBE DEM are the largest in Pamir (up to 3000 m), while in all other regions these differences are considerably lower (up to 600 m). Nevertheless, the area-averaged mass balance over 1961-2000, when only DEM GLOBE elevations are used for these regions, is within the ±0.15 m yr^{-1} from the reference estimates except for Svalbard. Here the difference in area-averaged mass balance is 0.41 m yr^{-1}, leading to a bias of -0.02 m SLE in the global volume loss by the end of 2100. This largest bias of -0.02 m SLE due to extraction of elevations from GLOBE DEM does not exceed our total uncertainty range (±0.04 m SLE) discussed in this section.

3.6 Other uncertainties

Our estimates include a number of additional uncertainties which are discussed here, but which are currently difficult to quantify. Following previous studies[2,9,21,22,23] we assume all glacier mass loss to instantaneously contribute directly to sea-level rise, and ocean area to remain constant. However, for more accurate estimates of SLE one should correct for the glacier meltwater that flows into aquifers and enclosed basins rather than to the ocean, isostatic adjustment of the land surface and the ocean floor to changes in ice and water loading, migration of grounding lines and shorelines, as well as changes in ocean area. In addition we do not account for the presence of floating and grounded ice below ice level. Except for a small effect on seawater density caused by reduction of salinity upon ice melting, the melting of floating ice does not contribute to sea-level. Grounded ice below sea-level already displaces ocean water. Therefore, we are possibly overestimating sea-level rise for these glaciers. However, quantitative assessments of the fraction of ice floating or below sea-level are not available on larger scales at this time.

Another uncertainty lies in the assumption that the parameters of the mass-balance model and the transfer functions remain constant under future climate conditions, although parameters can be expected to vary (e.g. ref. 41). The relationship between air temperature and melt may change when, for example, changes in melt rates are driven by other variables than temperature. Some studies have pointed out the importance of variations in solar radiation as drivers of glacier mass changes[41]. Also, the performance of the temperature-index model is limited for tropical glaciers (e.g. for South America 0°-30°S) where variations in radiation are the dominant driver of glacier mass changes. Hence, a more physically correct approach would be to apply a physically-based energy mass balance model, accounting for all components of the energy balance at the glacier surface. However, the added model complexity is most likely compromised by large uncertainties in the necessary input data both for the recent past and for the future. Currently, the performance of GCM in simulating surface radiation fluxes is insufficient[42] and some form of GCM downscaling (dynamical or statistical) will carry another spectrum of uncertainties.

Moreover, the model does not account explicitly for different ice temperature regimes. Compared to temperate glaciers, on polythermal glaciers some of the energy available at the glacier surface during the melt season will be consumed for warming the ice, and hence coefficients in the melt model can be different. Because the model calibration is performed mainly on temperate glaciers, the model parameters might not adequately simulate the response of polythermal glaciers to an air temperature increase. However, through inclusion of a few polythermal glaciers (for example from

Scandinavia) we indirectly account (at least partially) for this bias when deriving the model parameters.

Further uncertainty arises from possible errors in the observed elevation-dependent mass balances of the 36 glaciers which are used for deriving model parameters. Glacier-wide balances are often extrapolated from a sparse network of ablation stakes. In some cases, comparison between cumulative balances based on the glaciological method and geodetic balances has revealed large differences (e.g. ref. 43) indicating the potential of large errors in the reported annual mass-balance series. However, uncertainties are generally not quantified and reported.

Our results are sensitive to the choice of reference climate data used for the model calibration and for the bias correction in GCM data. Here we used the ERA-40 dataset and a precipitation climatology which both carry biases in their representation of recent climate[16,17]. Also, our results may be sensitive to the choice of the baseline period used for model initialization. Analysis on one valley glacier showed that the choice of the baseline period plays a minor role when compared to the uncertainties pertaining to the choice of GCM forcing the model[27], however, further studies are needed to quantify this uncertainty on larger scales. Here, our choice of 1961-2000 for the baseline period was constrained by the spatial and temporal availability of quality controlled mass balance observations and temporal availability of the reference climate data. Many mass-balance series were too short to allow for a robust analysis of the effect of choosing different baseline periods.

Supplementary Tables

Supplementary Table S1 Projected volume loss of mountain glaciers and ice caps, for different studies. Superscript *excl* and *incl* denote estimates excluding and including, respectively, mountain glaciers and ice caps around the Greenland and Antarctic ice sheets.

Study	Period	SLE^{excl} (m)	SLE^{incl} (m)
This study	2001-2100	0.099 ± 0.030	0.124 ± 0.037
Meehl *et al.*, 2007 (ref. 9)	2001-2100		0.07 – 0.17
Meier *et al.*, 2007 (ref. 1) *no acceleration*	2001-2100		0.104 ± 0.025
with acceleration	2001-2100		0.240 ± 0.128
Raper and Braithwaite, 2006 (ref. 10)	2001-2100	0.046, 0.051	
Van de Wal and Wild, 2001 (ref. 44)	2001-2070	0.057	
Gregory and Oerlemans, 1998 (ref. 45)	1990-2100	0.132, 0.182	

Supplementary Table S2 Model identification, originating group, and atmospheric resolution. In this study only run 1 is used from each GCM.

	Model	Center and location	Resolution
1	CGCM3.1(T63)	Canadian Centre for Climate Modelling and Analysis (Canada)	T63 L31
2	CNRM-CM3	Meteo-France, Centre National de Recherches Meteorologiques (France)	T42 L45
3	CSIRO-Mk3.0	CSIRO Atmospheric Research (Australia)	T63 L18
4	GFDL-CM2.0	US Dept. of Commerce, NOAA, Geophysical Fluid Dynamics Laboratory (USA)	N45 L24
5	GISS-ER	NASA/Goddard Institute for Space Studies (USA)	72×46 L17
6	IPSL-CM4	Institut Pierre Simon Laplace (France)	96×72 L19
7	ECHAM/MPI-OM	Max Plank Institute for Meteorology (Germany)	T63 L32
8	CCSM3	National Center for Atmospheric Research (USA)	T85 L26
9	PCM	National Center for Atmospheric Research (USA)	T42 L18
10	UKMO-HadCM3	Hadley Centre for Climate Prediction and Research, Met Office (UK)	96×72 L19

DOI: 10.1038/NGEO1052

Supplementary Table S3 36 glaciers with observed seasonal mass balance profiles used for the model calibration: glacier name, location (country, latitude, longitude), surface area, S (km^2), mean elevation, h (m), continentality index, CI (K), annual sum of precipitation, P_{ann} (mm), and the calibrated values of model parameters: lr_{ERA} (K (100m)$^{-1}$), lr (K (100m)$^{-1}$), f_{snow}(mm w.e. d^{-1} ^{o}C^{-1}), f_{ice} (mm w.e. d^{-1} ^{o}C^{-1}), k_P, d_{prec}((100m)$^{-1}$), and T_{snow} (^{o}C).

	Glacier	Country	Lat	Lon	S	h	CI	P_{ann}	lr_{ERA}	lr	f_{snow}	f_{ice}	k_P	d_{prec}	T_{snow}
1	Ålfotbreen	Norway	61.75°N	5.67°E	4.46	1150	13.6	2383	-0.55	-0.69	3.8	5.4	2.6	0.000	1.8
2	Austdalsbreen	Norway	61.80°N	7.35°E	11.86	1477	16.2	1399	-0.67	-0.44	3.2	6.3	3.1	0.114	1.0
3	Austre Brøggerbreen	Norway	78.83°N	11.50°E	6.12	325	14.7	363	-0.52	-0.33	7.2	9.0	2.6	0.000	0.8
4	Austre Okstindbreen	Norway	66.23°N	14.37°E	14.01	1220	19.2	1561	-0.77	-0.57	7.1	8.8	2.5	0.072	1.0
5	Bench	Canada	51.43°N	124.92°W	10.51	2150	19.0	1066	-0.66	-0.21	6.6	8.3	3.5	0.051	1.0
6	Blåisen	Norway	68.33°N	17.85°E	2.18	1025	19.8	820	-0.72	-0.59	3.9	4.9	4.6	0.153	1.7
7	Bondhusbreen	Norway	60.03°N	6.33°E	10.47	1048	16.4	2440	-0.82	-0.36	7.7	10.7	1.8	0.105	0.8
8	Bridge	Canada	50.82°N	123.57°W	48.44	1900	19.8	1093	-0.93	-0.27	5.5	6.9	2.8	0.104	0.4
9	Djankuat	Russia	43.20°N	42.77°E	2.90	3150	22.7	996	-0.64	-0.30	7.1	10.5	4.8	0.066	2.0
10	Engabreen	Norway	66.67°N	13.85°E	37.93	900	18.2	2010	-0.53	-0.43	3.9	6.2	3.2	0.080	0.6
11	Golubina	Kirghizstan	42.45°N	74.50°E	6.28	3800	23.7	399	-0.59	-0.33	4.6	8.5	5.6	0.122	1.2
12	Gråsubreen	Norway	61.65°N	8.60°E	2.34	2050	18.1	517	-0.75	-0.65	6.3	8.3	3.4	0.069	0.0
13	Hansebreen	Norway	61.75°N	5.68°E	3.32	1124	13.6	2383	-0.75	-0.72	5.2	6.5	2.6	0.039	0.5
14	Hellstugubreen	Norway	61.57°N	8.43°E	3.09	1775	18.1	644	-0.60	-0.41	3.1	6.2	3.7	0.094	1.5
15	Høgtuvbreen	Norway	66.45°N	13.65°E	2.60	888	17.5	1959	-0.66	-0.26	6.2	7.8	2.9	0.078	1.2
16	Jostefonn	Norway	61.42°N	6.58°E	3.81	1295	15.5	1578	-0.84	-0.42	5.5	8.0	3.3	0.038	0.5
17	Nigardsbreen	Norway	61.72°N	7.13°E	46.63	1150	16.3	1399	-0.75	-0.47	5.5	6.9	2.9	0.047	2.0
18	Peyto	Canada	51.67°N	116.58°W	13.05	2550	23.3	753	-0.84	-0.81	3.9	4.9	3.2	0.062	0.5
19	Place	Canada	50.43°N	122.60°W	3.79	2200	19.6	1689	-0.69	-0.53	2.4	4.9	1.9	0.071	0.9
20	Ram River	Canada	51.85°N	116.18°W	1.83	2795	23.3	605	-0.77	-0.18	6.3	9.7	4.3	0.173	0.6
21	Rembesdalskåka	Norway	60.53°N	7.37°E	17.18	1475	18.2	1125	-0.54	-0.33	2.9	5.8	3.7	0.122	1.9
22	Riukojietna	Sweden	68.08°N	18.08°E	4.62	1310	21.2	703	-0.50	-0.24	2.6	5.2	3.6	0.120	0.9
23	Sentinel	Canada	49.90°N	122.98°W	1.57	1800	17.9	3004	-1.00	-0.60	5.3	8.2	1.9	0.183	0.9
24	South Cascade	USA	48.37°N	121.05°W	1.74	1950	19.1	1713	-0.73	-0.94	2.5	5.0	2.1	0.000	1.4
25	Storbreen	Norway	61.57°N	8.13°E	5.20	1775	17.8	644	-0.70	-0.44	4.9	8.5	6.0	0.096	1.2
26	Storsteinfjellbreen	Norway	68.22°N	17.92°E	6.03	1405	21.2	820	-0.64	-0.43	4.7	5.9	4.9	0.074	1.8
27	Svartisheibreen	Norway	66.58°N	13.75°E	5.48	1098	18.2	2010	-0.67	-0.38	6.0	9.8	2.6	0.050	2.0
28	Sykora	Canada	50.87°N	123.58°W	25.35	2100	19.8	1093	-0.97	-0.57	7.0	8.8	3.0	0.054	0.0
29	Trollbergdalsbreen	Norway	66.72°N	14.45°E	1.79	1100	18.7	1679	-0.77	-0.39	5.5	6.9	2.7	0.088	2.0
30	Tsentralniy Tuyuksu	Kazakhstan	43.00°N	77.10°E	3.05	3805	22.9	574	-0.60	-0.38	5.9	7.5	5.6	0.128	1.5
31	Tunsbergdalsbreen	Norway	61.60°N	7.05°E	47.18	1243	16.3	1399	-0.73	-0.27	5.9	8.6	3.3	0.059	0.5
32	Vermuntgletscher	Austria	46.85°N	10.13°E	2.24	2850	18.2	1041	-0.56	-0.56	3.7	7.0	1.8	0.005	1.3
33	Woolsey	Canada	51.12°N	118.05°W	3.89	2298	23.5	1275	-0.85	-0.42	5.1	6.5	3.5	0.065	0.7
34	Zavisha	Canada	50.80°N	123.42°W	6.49	2250	19.8	901	-0.58	-0.38	2.5	4.0	3.4	0.095	2.0
35	Helm	Canada	50.00°N	123.00°W	2.25	2000	17.9	1689	-0.69	-0.10	3.0	5.9	2.4	0.241	0.0
36	Tiedemann	Canada	51.33°N	125.05°W	34.87	2850	19.0	1335	-0.34	-0.34	4.5	5.7	2.8	0.091	1.7

Supplementary Table S4 41 glacier regions used for the model initialization: Longitude, latitude, number of WGI-XF glaciers per region, period of annual mass balance observations from ref. 14 (D&M05). *B* (D&M05) is the area-averaged mass balance (m yr^{-1}) from ref. 14 averaged over the observation period, *B* (init.) is our modeled mass balance averaged over the same observation period, and *B* (61-00) is the modeled balance averaged over the period 1961-2000. lr_{ERA} (K (100 m)$^{-1}$) is the statistical lapse rate tuned to yield agreement within ±0.1 m yr^{-1} between modeled mass balance and *B* (D&M05). $\Delta B/\Delta T$ (m yr^{-1} K^{-1}) and $\Delta B/\Delta P$ (m yr^{-1}), are the modeled mass balance sensitivities to temperature and precipitation change, respectively.

	Glacier region	Lat	Lon	Number of WGI-XF glaciers	Period D&M05	*B* D&M05	*B* init.	*B* 61-00	lr_{ERA}	$\Delta B/\Delta T$	$\Delta B/\Delta P$
1	Alps	45-47N	6E-11E	5,165	1961-2000	-0.11	-0.20	-0.20	-0.60	-0.78	0.19
2	Scandinavia	61-68N	7-18E	2,408	1961-2000	0.28	0.21	0.21	-0.92	-0.79	0.23
3	Iceland	64-65N	16-20W	64	1989-2000	-0.16	-0.13	0.11	-0.06 *	-1.06	0.19
4	Caucasus	42.5-43.5N	43-45E	1,522	1961-2000	-0.21	-0.27	-0.27	-0.66	-0.71	0.16
5	Altai	51-52N	89-91E	1,854	1961-2000	-0.08	-0.10	-0.14	-0.81	-0.49	0.07
6	Kamchatka	53-55N	158-160N	398	1971-1997	-0.08	-0.15	-0.15	-0.78	-0.50	0.12
7	Suntar-Khayata Range	62-62.5N	140-142E	430	1961-1969	-0.10	-0.11	-0.39	-0.73	-0.66	0.07
8	Dzhungaria	43N	80E	1,482	1961-1999	-0.07	-0.10	-0.10	-0.78	-0.49	0.08
9	Himalaya	28-30N	78-92E	27,761	1961-1999	-0.41	-0.44	-0.45	-0.36	-0.68	0.11
10	Kun-Lun	36-37N	77-87E	11,633	1961-1999	0.10	0.19	0.17	-0.65	-0.17	0.05
11	Tibet	30-33N	80-95E	2,140	1961-1999	0.30	0.21	0.21	-0.59	-0.54	0.08
12	Pamir	37-39N	72-75E	13,260	1961-1999	-0.26	-0.30	-0.32	-0.64	-0.37	0.08
13	Quilanskan	37-39N	95-100E	3,165	1961-1999	0.01	-0.03	-0.06	-0.69	-0.35	0.05
14	Gongga	30N	97E	1,664	1961-1999	-0.25	-0.29	-0.33	-0.47	-0.71	0.10
15	Tien Shan	41-43N	76-82E	15,004	1961-2000	-0.35	-0.41	-0.43	-0.63	-0.42	0.07
16	Axel Heiberg	78-80N	87-93W	1,084	1961-2000	-0.13	-0.16	-0.16	-0.33	-0.41	0.03
17	Devon ice cap	75-76N	80-83W	645	1961-2000	-0.07	-0.11	-0.11	-0.37	-0.48	0.03
18	Ellesmere Island	78-83N	70-85W	117	1961-2000	-0.05	-0.09	-0.09	-0.31	-0.41	0.02
19	Svalbard	77-81N	11-26E	2,195	1961-2000	-0.11	-0.04	-0.04	-0.32	-0.71	0.08
20	Polar Ural	68N	65E	70	1961-1981	-0.13	-0.13	-0.25	-1.30	-0.59	0.14
21	Severnaya Zemlya	78-81N	95-105E	385	1961-1999	-0.04	-0.01	-0.02	0.34 *	-0.56	0.04
22	Novaya Zemlya [a]	76°N	62°05'E	685	1969-1971	0.14	-0.01	0.01	0.23 *	-0.70	0.06
23	Franz Josef Land	80°06'N	52°48'E	995	1961-1993	-0.07	-0.01	-0.04	0.40 *	-0.63	0.04
24	Brooks & Arctic Ocean	68N	150-160W	132	1969-1972	-0.19	-0.10	-0.42	-0.62	-0.55	0.05
25	Alaska Range	62-63N	150-153W	446	1966-2000	-0.33	-0.40	-0.38	-0.73	-0.38	0.05
26	Kenai Mountains	60-61N	145-148W	1	1965-2000	-0.25	-0.29	-0.29	-0.85	-0.75	0.14
27	Chugach [a]	61-62N	146-149W	403	1978-1980	0.36	-0.22	-0.22	-0.77	-0.36	0.05
28	St. Elias	58-61N	134-142W	1,425	1961-2000	-0.93	-0.90	-1.01	-0.50	-0.60	0.07
29	Coast	56-59.5N	132-135W	2,978	1961-2000	0.36	0.28	0.28	-0.81	-0.46	0.13
30	Rookies & Coast	49-60N	116-130W	4,908	1961-2000	-0.48	-0.51	-0.51	-0.65	-0.94	0.25
31	Olympic	48N	123W	256	1961-1999	-0.12	-0.20	-0.20	-0.70	-0.98	0.27
32	North Cascades	48.5N	121W	743	1961-2000	-0.34	-0.40	-0.40	-0.77	-0.77	0.27
33	Sierra Nevada [a]	38N	119W	429	1967-1969	0.38	-0.17	-0.17	-0.51	-0.55	0.15
34	South America I	02-20S	69-80W	4,479	1992-2000	-0.66	-0.75	-0.58	-0.56	-0.95	0.12
35	South America II	20-45S	73-75W	1,233	1976-2000	-0.31	-0.30	-0.31	-0.59	-0.41	0.09
36	S. & N. Patagonia [a]	46-54S		1,421	1996-1998	0.15	-0.79	-0.72	-0.63	-0.58	0.04
37	New Zealand	43-44S	170-171E	3,122	1970-1975	-2.38	-2.45	-1.74	-0.62	-1.24	0.15
38	Greenland	54-55S	36-37W	5,017	1961-2000	-0.12	-0.17	-0.17	0.29 *	-0.55	0.10
39	Sub-Antarctic islands	60-85N	20-70W	221	1967-1971	-0.2	-0.23	-0.09	-0.59 *	-1.21	0.11
40	Antarctica [b]	60-150W	65-72S	340	1971-1975	-0.03	-0.41	-0.41	0.00 *	-0.77	0.06
41	North & East Asia [c]			1,187			-0.20	-0.20	-0.95	-0.51	0.11

DOI: 10.1038/NGEO1052

Footnotes for Supplementary Table S4:

[a] These glacier regions have insufficiently long data records in ref. 14 (< 4 years) to initialize the model. Therefore we use the following procedure: For Novaya Zemlya the reference estimate is assumed the same as for Severnaya Zemlya; for Chugach the reference is Kenai Mountains, for Sierra Nevada the reference is the global mass balance (-0.27 m yr^{-1}), and for S. and N. Patagonia the reference estimate is -0.85 m yr^{-1} taken from ref. 32, for the period 1975-2000.

[b] For Antarctica we used the reference estimate of -0.40 m yr^{-1} for the period 1961-2004, as a mid-range estimate between refs 14 and 23.

[c] This region contains the remaining WGI-XF glaciers, which do not belong to any glacier region of ref. 14. These ice masses are scattered over North and East Asia. We adopt the global mass balance (-0.27 m yr^{-1}) as a reference estimate.

* More complex tuning is performed since adjustment of only one model parameter, lr_{ERA}, resulted in too large variances of seasonal and net mass balances of WGI-XF glaciers within the region. Therefore, we apply spatially differentiated adjustment of lr_{ERA} within the glacier region or modified another model parameter (precipitation correction factor, k_P). The following model parameters are adopted:
- Iceland: for ice caps with area > 500 km^2, k_P=1.
- Severnaya Zemlya: for mountain glaciers lr_{ERA} =-0.60 K $(100m)^{-1}$; for ice caps k_P=1.
- Novaya Zemlya: for mountain glaciers lr_{ERA}= -0.15 K $(100m)^{-1}$; for ice caps k_P=1.
- Franz Josef Land: For mountain glaciers lr_{ERA}=-0.05 K $(100m)^{-1}$ and k_P=2; for ice caps k_P=1.
- Greenland: lr_{ERA} is tuned independently on 4 subsections. Besides the value of lr_{ERA} in the table, the other three values for lr_{ERA} (K $(100m)^{-1}$) are: -0.28, -0.05 and -0.45; k_P=1.5.
- Sub-Antarctic islands: lr_{ERA} is tuned independently on 3 subsections. Besides the value of lr_{ERA} in the table, the other two values for lr_{ERA} (K $(100m)^{-1}$) are: -0.10 and -0.30.
- Antarctica: k_P=0.8.

For regions where precipitation climatology[17] is not available we use precipitation from ERA-40 reanalysis[16].

Supplementary Table S5 Mass balance model parameters tuned on 36 glaciers: parameters' initial range allowed in the optimization algorithm, mean and standard deviation, σ, transfer functions derived from multiple regression analysis and corresponding coefficient of determination r^2. lr_{ERA} is the statistical lapse rate, i.e. the bias correction between the temperature from ERA-40/GCM in the grid cell covering a glacier and the temperature at the highest altitude of the glacier, lr is the lapse rate along the glacier surface, $f_{snow/ice}$ is the degree-day factor for snow and ice, respectively, k_P is the precipitation correction factor, d_{prec} the precipitation gradient, i.e. the precipitation change in % per elevation increase in m, T_{snow} is the threshold temperature that discriminates snow from rain precipitation, h (m) is mean glacier elevation, CI (K) is continentality index, and P_{ann} (mm) is annual sum of precipitation. $\Delta B/\Delta T$ (m yr^{-1} K^{-1}) and $\Delta B/\Delta P$ (m yr^{-1}) are mass balance sensitivities to temperature and precipitation changes, respectively (see Equations 8 and 9 for details).

Parameter	Initial range	Mean	σ	Transfer function	r^2
$lr_{ERA}\left[\frac{K}{100m}\right]$	-1.00 -0.01	-0.69	0.14	-	-
$lr\left[\frac{K}{100m}\right]$	-1.00 -0.01	-0.44	0.18	-	-
$f_{snow}\left[\frac{mm\ w.e.}{d\ ^\circ C}\right]$	2.00 8.00	4.92	1.54	$f_{snow} = -0.856 - 5.175\ \frac{\Delta\overline{B}}{\Delta T} - 6.804\ \frac{\Delta\overline{B}}{\Delta P} + +0.217\ CI - 7.5\times10^{-4}\ \overline{h}$	0.33
$f_{ice}\left[\frac{mm\ w.e.}{d\ ^\circ C}\right]$	4.00 12.00	7.17	1.72	$f_{ice} = 0.539 - 6.067\ \frac{\Delta\overline{B}}{\Delta T} - 6.804\ \frac{\Delta\overline{B}}{\Delta P} + +0.184\ CI - 4.3\times10^{-4}\ \overline{h}$	0.33
k_P	0.00 20.00	3.28	1.07	$k_P = 3.485 + 7.164\ \frac{\Delta\overline{B}}{\Delta P} - 1.77\times10^{-3}\ P_{ann} - -2.32\times10^{-4}\ \overline{h}$	0.53
$d_{prec}\left[\frac{1}{100m}\right]$	0.00 0.90	0.08	0.05	-	-
$T_{snow}\left[^\circ C\right]$	0.00 2.00	1.11	0.61	-	-

Footnotes for Supplementary Table S5:

Transfer functions for model parameters (f_{snow}, f_{ice} and k_P) contain mass balance sensitivities to temperature and precipitation change ($\Delta B/\Delta T$ and $\Delta B/\Delta P$) which are determined with the following functions:

$$\frac{\Delta\overline{B}}{\Delta T} = -0.980 + 0.014CI - 1.4\times10^{-4} P_{ann} \quad (r^2=0.34)$$

$$\frac{\Delta\overline{B}}{\Delta P} = 0.053 + 0.002CI - 1.2\times10^{-4} P_{ann} \quad (r^2=0.74)$$

DOI: 10.1038/NGEO1052

Supplementary Table S6 Total glacierized area[12] for 19 regions defined by a rectangle with coordinates for NW corner and SE corner (Fig. S1). Modelled area-averaged mass balance B (m w.e yr^{-1}) for each region averaged over 1961-2000, also expressed in sea-level equivalent (SLE), projected average rates of SLE over 2001-2100, and volume change ΔV (mm SLE) by 2100. ΔV is given as multi-model mean ±1 standard deviation from the ensemble of 10 GCMs listed in Table S2.

Region	Geographical coordinates		Area	B	SLE	SLE	ΔV
				1961-2000		2001-2100	
	NW corner	SE corner	km^2	m yr^{-1}	mm yr^{-1}	mm yr^{-1}	mm SLE
1 Svalbard	83°N 10°E	77°N 36°E	36,506	-0.04	0.005	0.139	13.9 ± 3.7
2 Scandinavia	71°N 5°E	60°N 33°E	3,057	0.21	-0.002	0.002	0.2 ± 0.2
3 European Alps	48°N 2°W	43°N 13°E	3,045	-0.20	0.002	0.004	0.4 ± 0.1
4 Franz Josef Land	82°N 45°E	80°N 65°E	13,739	-0.04	0.001	0.029	2.9 ± 1.5
5 Novaya Zemlya	77°N 53°E	73°N 68°E	23,645	0.01	0.000	0.073	7.3 ± 3.5
6 Severnaya Zemlya	82°N 79°E	76°N 107°E	19,397	-0.02	0.001	0.031	3.1 ± 2.1
7 Caucasus	44°N 40°E	36°N 52°E	1,397	-0.27	0.001	0.001	0.1 ± 0.0
8 North and East Asia[1]	72°N 59°E	48°N 179°E	2,902	-0.18	0.002	0.001	0.1 ± 0.1
9 High Mountain Asia	48°N 67°E	28°N 103°E	114,330	-0.24	0.077	0.033	3.3 ± 4.8
10 Alaska[2]	70°N 161°W	57°N 132°W	79,260	-0.49	0.107	0.257	25.7 ± 6.9
11 W. Canada and W. US	76°N 132°W	37°N 109°W	21,480	-0.48	0.028	0.024	2.4 ± 0.3
12 Arctic Canada	84°N 101°W	58°N 63°W	146,690	-0.13	0.054	0.270	27.0 ± 12.4
13 Iceland	71°N 24°W	64°N 8°W	11,005	0.11	-0.003	0.044	4.4 ± 2.8
14 South America I	7°N 79°W	27°S 67°W	7,060	-0.58	0.011	0.002	0.2 ± 0.1
15 South America II	32°S 75°W	55°S 69°W	29,640	-0.69	0.057	0.074	7.4 ± 1.0
16 New Zealand	39°S 167°E	45°S 177°E	1,156	-1.74	0.006	0.001	0.1 ± 0.0
17 Greenland	85°N 13°W	58°N 80°W	54,400	-0.17	0.025	0.036	3.6 ± 2.0
18 Sub-Antarctic islands	49°S 0°W	60°S 0°E	3,740	-0.09	0.001	0.005	0.5 ± 0.2
19 Antarctica	60°S 0°W	85°S 0°E	169,000	-0.41	0.191	0.213	21.3 ± 12.2
Total			741,448	-0.27	0.562	1.240	124 ± 37

[1] Additional box: NW corner: 78°N 118°E; SE corner: 75°N 158°E.

[2] Including northwestern Canada

Supplementary Figures

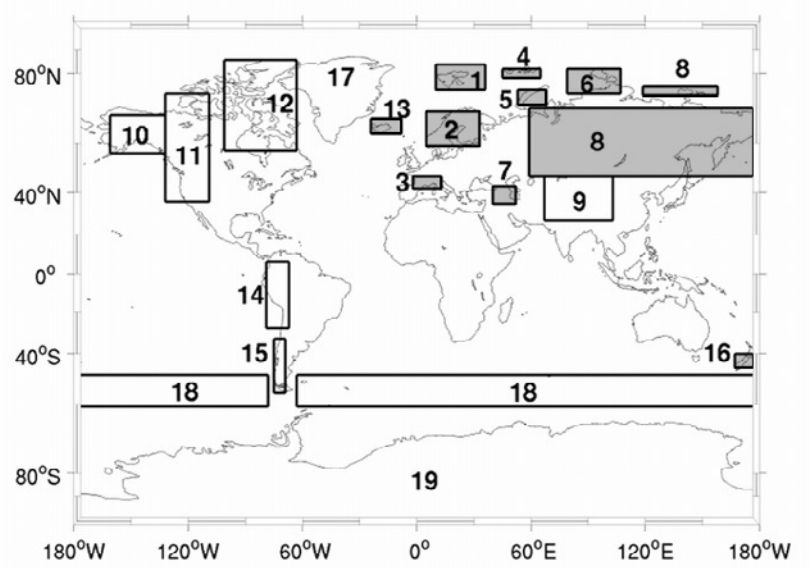

1 Svalbard
2 Scandinavia
3 European Alps
4 Franz Josef Land
5 Novaya Zemlya
6 Severnaya Zemlya
7 Caucasus
8 North and East Asia
9 High Mountain Asia
10 Alaska
11 West Canada and West US
12 Arctic Canada
13 Iceland
14 South America I (0°-30°S)
15 South America II (30°-55°S)
16 New Zealand
17 Greenland
18 Sub-Antarctic Islands
19 Antarctica

Supplementary Figure S1 Location of the 19 regions containing mountain glaciers and ice caps. Shaded rectangles denote 10 regions with complete glacier inventories. Note that region 12 does not include any glaciers in Greenland. Regions 17 (Greenland) and 19 (Antarctica) include all mountain glaciers and ice caps apart from the ice sheets. See Table S6 for coordinates of the rectangles.

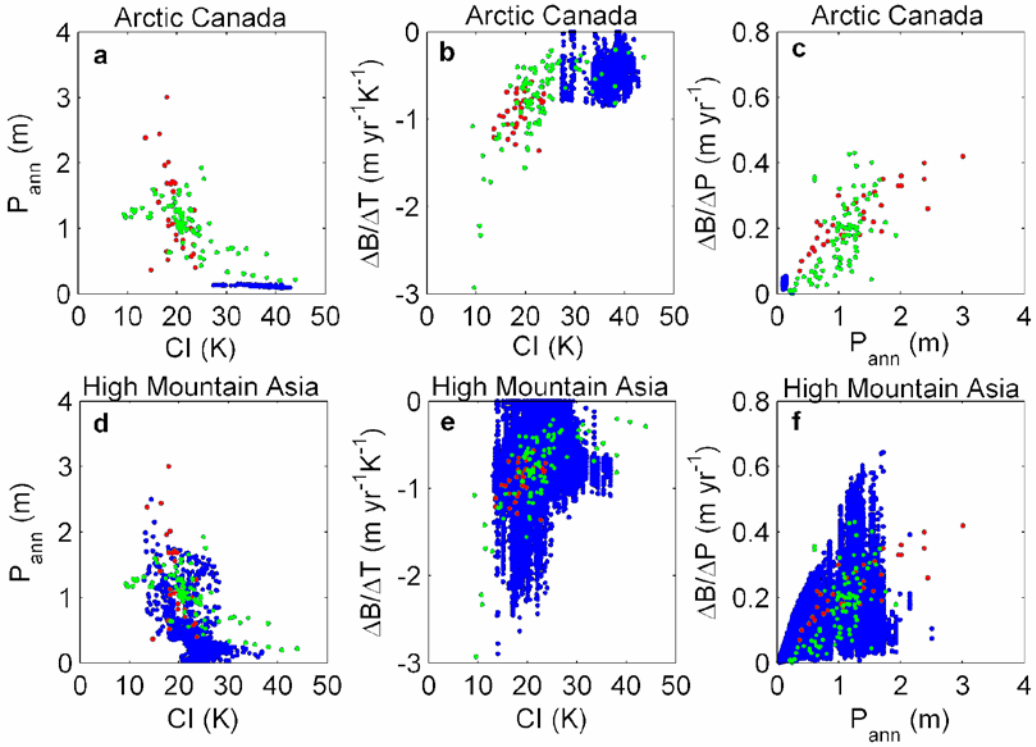

Supplementary Figure S2 Annual sum of precipitation, P_{ann}, versus continentality index, *CI*, (a, d) and mass balance sensitivities to temperature increase of 1 K, $\Delta B/\Delta T$, and 10% increase in precipitation, $\Delta B/\Delta P$, versus *CI* (b, e) and P_{ann} (c, f). Blue dots represent all WGI-XF glaciers, red dots represent the 36 glaciers used in the model calibration (Table S3) and green dots are 88 glaciers from ref. 23.

DOI: 10.1038/NGEO1052

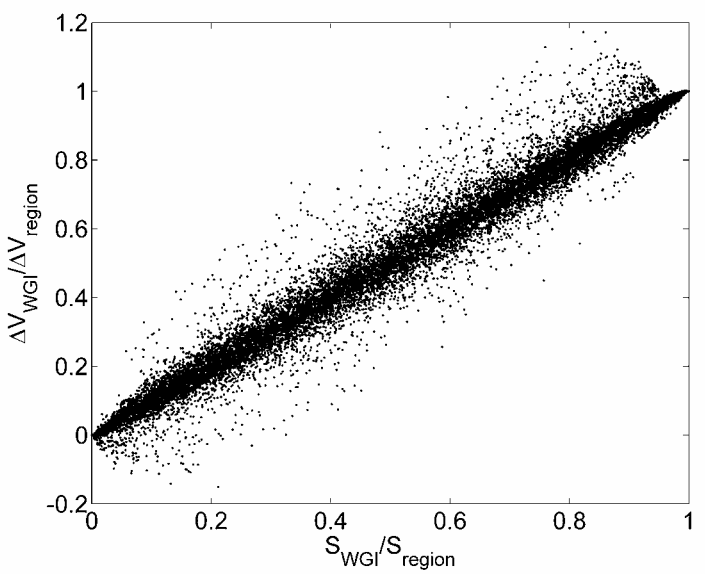

Supplementary Figure S3 Ratio between the 21st century volume change of all WGI-XF glaciers in each region, ΔV_{WGI}, and the total ice volume change in each region, ΔV_{region}, versus ratio between the area of all WGI-XF glaciers in each region, S_{WGI}, and the total ice area in each region, S_{region}.

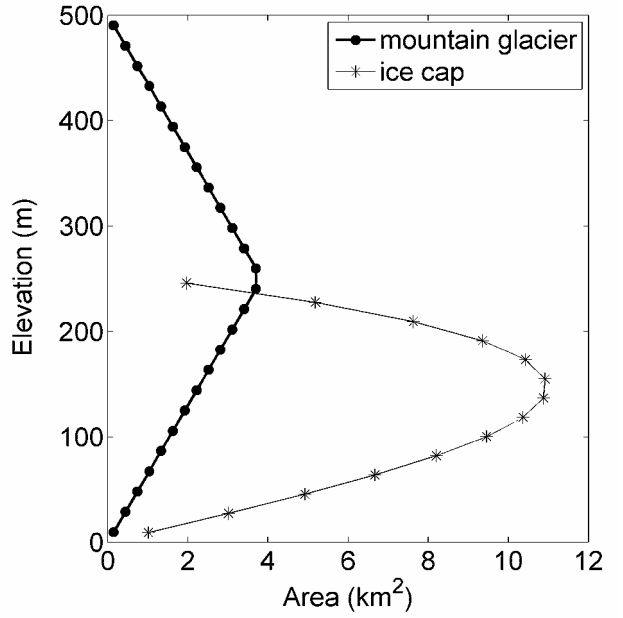

Supplementary Figure S4 Example for area-altitude distribution of an ice cap (S=100 km^2) and a mountain glacier (S=50 km^2) computed for 20 m elevation bands.

Supplementary References
(for references 1 to 27 see main text)

28. Elsberg, D. H., Harrison, W. H., Echelmeyer, K. A. & Krimmel, R. M. Quantifying the effects of climate and surface change on glacier mass balance. *J. Glaciol*. **47**(159), 649-658 (2001).
29. Oerlemans, J. & Fortuin, J. P. F. Sensitivity of glaciers and small ice caps to greenhouse warming. *Science* **258**, 115-117 (1992).
30. Braithwaite, R. J. & Zhang, Y. Modelling changes in glacier mass balance that may occur as a result of climate changes. *Geogr. Ann*. **81A**(4), 489-496 (1999).
31. Holmlund, P. & Schneider, T. The effect on continentality on glacier response and mass balance. *Ann. Glaciol*. **24**, 272-276 (1997).
32. Rignot, E., Rivera, A. & Cassasa, G. Contribution of the Patagonia Icefields of South America to sea level rise. *Science* **302**, 434-437 (2003).
33. Paul, F. & Heaberli, W. Spatial variability of glacier elevation changes in the Swiss Alps obtained from two digital elevation models, *Geophys. Res. Lett*. **35**, L21502 (2008).
34. Schiefer, E., Menounos, B. & Wheate, R. Recent volume loss of British Columbia glaciers, Canada, *Geophys. Res. Lett*. **34**, L16503 (2007).
35. Bahr, D. B. Global distributions of glacier properties: A stochastic scaling paradigm. *Water Resour. Res.* **33(7)**, 1669-1679 (1997).
36. Chen, J. & Ohmura, A. Estimation of Alpine glacier water resources and their change since the 1870's. International Association of Hydrological Science Publication 193 (Symposium at Lausanne 1990 – Hydrology in Mountainous Regions. I – Hydrological Measurements; the Water Cycle) 127-135 (1990).
37. Berthier, E., Schiefer, E., Clarke, G. K. C., Menounos, B. & Rémy, F. Contribution of Alaskan glaciers to sea-level rise derived from satellite imagery. *Nat. Geosci.* **3**, 92-95 (2010).
38. Bolch, T., Menounos, B. & Wheate, R. Landsat-based inventory of glaciers in western Canada, 1985-2005. *Remote Sens. Environ.* **114**, 127-137 (2010).
39. <http://www.glaciers.us/States-Glaciers>
40. Bevington, P. R. *Data Reduction and Error Analysis for the Physical Sciences*, (McGraw-Hill, New York, 1969).
41. Huss, M., Funk, M. & Ohmura, A. Strong Alpine melt in the 1940s due to enhanced solar radiation. *Geophys. Res. Lett*. **36**, L23501 (2009).
42. Randall, D. A. *et al*. Climate Models and their Evaluation. In: Solomon, S. *et al.* (eds) *IPCC Climate Change 2007: The Physical Science Basis* (Cambridge Univ. Press, Cambridge, 2007).
43. Haug, T., Rolsrad, C., Elvehøy, H., Jackson, M. & Maalen-Johansen, I. Geodetic mass balance of the western Svartisen ice cap, Norway, in the periods 1968-1985 and 1985-2002. *Ann. Glaciol*. **50(50)**, 119-125 (2009).
44. Van de Wal, R. S. W. & Wild, M. Modelling the response of glaciers to climate change by applying volume-area scaling in combination with a high resolution GCM. *Clim. Dyn.* **18(3-4)**, 359-366 (2001).
45. Gregory, J. M. & Oerlemans, J. Simulated future sea-level rise due to glacier melt based on regionally and seasonally resolved temperature changes. *Nature* **391**, 474-476 (1998).